Materials Science and Engineering B 284 (2022) 115851

Contents lists available at ScienceDirect

Materials Science & Engineering B

journal homepage: www.elsevier.com/locate/mseb

Azadirachta indica leaf extract mediated biosynthesized rod-shaped zinc oxide nanoparticles for in vitro lung cancer treatment

Nutan Rani [a], Kavita Rawat [b], Mona Saini [a], Sapna Yadav [a], Anju Shrivastava [b], Kalawati Saini [a,*], Dipak Maity [c,d,*]

[a] Department of Chemistry, Miranda House, University of Delhi, Patel Chest Marg, New Delhi 110007, India
[b] Department of Zoology, University of Delhi, North Campus, New Delhi 110007, India
[c] Department of Chemical Engineering, University of Petroleum and Energy Studies, Bidholi, Dehradun 248007, India
[d] School of Health Sciences & Technology, University of Petroleum and Energy Studies, Bidholi, Dehradun 248007, India

ARTICLE INFO

Keywords:
Azadirachta indica
Zinc oxide nanoparticles
Apoptosis
Lung cancer treatment
Biosynthesis using Neem leaf extract

ABSTRACT

In this work, ZnO nanoparticles (NPs – L5 and L10) are biosynthesized using 5 mL and 10 mL leaf extract of *Azadirachta indica*, respectively. As-prepared L5/L10 NPs revealed hexagonal wurtzite structure while their surface is attached with phytochemicals coating. FESEM micrographs confirmed 50 – 120 and 30 – 70 nm rod-shaped L5/L10 ZnO nanoparticles. DLS study showed hydrodynamic sizes 580.41/356.2 nm and zeta potential values of −47.17/−51.70 mV for L5/L10, respectively indicating their good colloidal stability. The anticancer activity of L5/L10 NPs is evaluated via MTT assay which confirmed that the cell viability of A549 cells is significantly reduced depending on the dosage of L5/L10 NPs. Moreover, IC_{50} values are obtained as 125.64 and 115.63 μg/mL for L5 and L10, respectively. Furthermore, flow cytometry reveals 88 % and 89.3 % arrest of the G1 phase of the cell cycle due to the anticancer effect of L5 and L10 NPs, respectively.

1. Introduction

Nowadays, the demand for metal oxide nanoparticles (MONPs) based nanotechnology has tremendously increased, particularly in the biomedical and pharmaceutical sectors. However, there is a mandate to synthesize biocompatible MONPs by cost-effective and eco-friendly strategies rather than utilizing conventional techniques such as sol–gel, hydrothermal method, laser ablation, microwave-assisted, ball milling and many other methods [1–6]. Therefore, plant extract mediated (using various plant parts) and microbe mediated (using bacteria, fungi and yeast) biosynthesis of nanoparticles has attracted huge attention due to their inexpensive and nontoxic nature [7–11]. Several MONPs such as NiO, Fe_2O_3, TiO_2, CuO, ZnO, Cr_2O_3, SnO_2, CdO and Eu_2O_3 MONPs with a variety of sizes and shapes have been naturally prepared via biosynthesis method [12–23]. Besides, plant extracts (obtained from leaf, bark, stem, flower, and root) consist of biomolecules/phytochemicals such as polyphenols, alkaloids, terpenoids, polysaccharides etc. can act as both reducing agents and capping/stabilizing agents in the biosynthesis approach.

Biosynthesized ZnO nanoparticles (NPs) are widely investigated in various applications particularly in antibacterial, antidiabetic, photocatalytic, anticancer and anti-inflammatory activities due to their unique physicochemical properties including chemical stability, low toxicity, wide bandgap (~3.37 eV, n-type semiconductor) and so on [24–30]. Cancer is a deadly disease due to uncontrollable growth/division of cells and the cause of death for the increased number of patients day by day. Among the different types of cancer (breast, lung, ovarian, prostate and so on), the death rate and prevalence of lung cancer are more frequent. Recently, nanomedicine is evolving as an alternative treatment for the prevention and cure of cancer to overcome side effects associated with clinically available chemotherapy, radiotherapy, and surgery techniques.

There are many reports available where biosynthesized ZnO NPs have been studied for their in vitro and in vivo anticancer activity [31–33]. It is reported that many phytochemicals are present in the *Azadirachta indica* (Neem tree) leaves [34,35]. Besides, phytochemicals present in Neem leaf have been proven to exhibit antimalarial, antiviral, antioxidant, antibacterial, antiulcer, antifungal and anticarcinogenic activities [36]. In this work, we have reported biosynthesis of rod-shaped ZnO NPs (L5 and L10) using 5 mL and 10 mL leaf extract of

* Corresponding authors.
E-mail addresses: kalawati.saini@mirandahouse.ac.in (K. Saini), dipakmaity@gmail.com (D. Maity).

https://doi.org/10.1016/j.mseb.2022.115851
Received 9 May 2022; Received in revised form 24 June 2022; Accepted 30 June 2022
Available online 18 July 2022

Azadirachta indica, respectively and evaluation of their anticancer activity on A549 lung cancer cells. Comparative studies of L5 and L10 NPs have been carried out to investigate their physicochemical properties and cell viability/morphology/apoptosis induction capacity on A549 cell lines using assays like MTT assay, crystal violet assay, and flow cytometry.

2. Materials and methods

All the required chemicals/reagents are of analytical grade and used without any further purification. Sodium hydroxide (NaOH) flakes and zinc sulphate heptahydrate ($ZnSO_4{\cdot}7H_2O$) were obtained from Central Drug House (P) Ltd - CDH, India whereas methanol and dimethyl sulfoxide (DMSO) were procured from SRL, India. A549 (human lung adenocarcinoma) cells were acquired from the National Cell Repository of Animal Cells (NCCS), Pune, India. MTT (3-(4, 5-dimethylthiazol-2-yl)-2, 5-diphenyltetrazolium bromide) and DMEM (Dulbecco's modified Eagle's medium) were obtained from Sigma Aldrich, USA. Acridine orange (AO), Propidium iodide (PI), Crystal violet, and RNase were procured from Bangalore Genei. FBS (Fetal bovine serum) was procured from Invitrogen. *Azadirachta indica* (Neem) leaves were acquired from the garden of the Department of Chemistry, University of Delhi.

2.1. Preparation of Azadirachta indica leaf extract

The fresh leaves of *Azadirachta indica* were washed several times with double distilled water to remove dust particles and any sticky materials. The cleaned leaves were dried at room temperature (RT) for a few hours and then finally dried in the oven for 2 h at 60 °C. After drying, leaves were chopped and powdered with the help of a mixer grinder. Next, 25 g of powdered leaves were taken in a beaker containing 100 mL of double-distilled water. The mixture was heated on a hot plate at 40 °C for 30 min and then cooled to RT. After cooling, the resultant leaf extract solution was filtered using Whatman filter paper and further utilised for the synthesis of ZnO nanoparticles.

2.2. Leaf extract mediated biosynthesis of ZnO NPs

A solution of zinc sulphate (0.2 M) was prepared in a beaker using double distilled water. To this solution, 5 mL of as-prepared leaf extract was added followed by dropwise addition of 1 M NaOH solution. The beaker containing the resultant mixture solution was heated on a magnetic hot plate at 40 °C for 120 min with constant stirring. After cooling to RT, the resultant white precipitate of ZnO NPs was washed with diluted alcohol several times. Finally, the washed ZnO NPs were dried in an oven for 6 h at 80 °C to obtain dry powders. The obtained ZnO powders are labelled as L5 and stored in a glass vial for further characterization. Likewise, ZnO NPs were synthesized using 10 mL of as-prepared leaf extract and labelled as L10.

2.3. Characterization of ZnO NPs

The phase purity, surface coatings, morphology (size and shape), particle size distribution and zeta potential of the as-synthesized ZnO nanoparticles (L5 and L10) were characterized by Powder X-ray Diffractometer (PXRD, D8 Discover, Bruker), UV–visible spectroscopy (UV–vis, Epoch™ Microplate Spectrophotometer, BIO-TEK®, USA), Fourier transform infrared spectroscopy (FTIR, 55-Spectrometer, Bruker, USA), thermogravimetric analysis (TGA, SF/1100, Mettler Toledo), field emission scanning electron microscope (FE-SEM, JSM-6610LV, JEOL Inc, Japan), and dynamic light scattering (DLS, nano-Partica SZ-100-Z, Horiba) techniques, respectively.

Powder X-ray diffraction (PXRD) pattern was recorded using an X-ray source (Cu K, $\lambda = 1.54056$ Å) in the 2θ range of 20°-80° and 0.0194°/sec scan rate. UV–vis absorption spectrum was recorded in the range of 200–800 nm and FT-IR spectrum was recorded using ATR (Attenuated total reflection) mode in a wavenumber range of 4000-400 cm^{-1}. TGA was performed to determine the percentage of weight loss in the temperature range of 35–800 °C with a heating rate of 10 °C/min. FESEM was operated at 20 kV accelerating voltage. DLS was used to determine the zeta potential and hydrodynamic size which respectively represent the colloidal stability and particle size distribution of the ZnO NPs dispersed in an aqueous suspension.

2.4. Cell culture

A549 (human lung adenocarcinoma) cells were cultured in DMEM medium supplemented with 10 % (v/v) heat-inactivated FBS (fetal bovine serum). Subsequently, all cultures were maintained at 37 °C in a humidified atmosphere containing 5% CO_2. Thereafter once every 2-3 days, the cells were passaged and a log of the arithmetic growth phase of the A549 cells was taken to perform different experiments namely MTT assay, crystal violet assay and flow cytometry analysis.

2.5. MTT and crystal violet assay

MTT (cytotoxicity) assay was carried out to determine the viability of A549 cells in presence of as-prepared ZnO NPs (L5/L10). The mitochondrial dehydrogenase enzymes present in the living cells can convert yellow soluble MTT to purple insoluble formazan precipitate as a result of cleavage of the tetrazolium ring. Briefly, 5×10^4 cells/well were seeded in 96 well plates and incubated overnight in DMEM to acclimatize (37 °C, 5% CO_2). After that, the cells were treated with different concentrations of ZnO NPs (100, 150, 200 and 250 μg/mL) in a CO_2 incubator at 37 °C for 24 h and 48 h. Then culture media was removed 4 h before termination and replaced with fresh medium (18 μL) and MTT solution (20 μL, 5 mg/mL in PBS). For the remaining 4 h, the plate was incubated in the dark humidified atmosphere in CO_2 in an incubator at 37 °C. Finally, the media was removed and the formed crystals of formazan were dissolved by adding DMSO (100 μL/well) and the optical density (OD) value was recorded using an Epoch^{tm} Microplate Spectrophotometer (BIO-TEK, USA) at 570 nm. IC_{50} (concentration at which 50 % inhibition occurs) was determined by the linear regression from the dose–response curve. Also, the following equation was used to calculate the % cell viability.

Percent cell viability = (OD value of treated sample/OD value of control sample) * 100

Crystal violet assay was a perforator to notice the morphology of A549 cells. Briefly, plating of A549 cells was done in a 6 well plate and left undisturbed overnight to adhere. Then adhered cells were treated with an IC_{50} dose of as-synthesized ZnO NPs (L5/L10) for 48 h. The medium was removed and cells were washed thrice with PBS. After that 100 % methanol was used to fix the cells for 1 min duration. Then crystal violet was used to stain the cells for less than 60 s duration. Next, the plate was washed thrice using tap water and then allowed to dry. Finally, stained cells were visualized under a normal inverted microscope (Nikon) at 200x magnification.

2.6. Acridine Orange/Propidium Iodide (AO/PI) staining

A double AO/PI staining procedure was used to know the effect of ZnO NPs on inducing apoptotic cell death of A549 cells. Briefly, plating of A549 cells was done in 6 well plates and incubated overnight to adhere. Then, the cells were exposed to a corresponding IC_{50} dose of as-synthesized ZnO NPs (L5/L10) for 48 h.

2.7. Flow cytometry for cell cycle analysis

Flow cytometry was performed to determine the quantification of DNA content. It is a widely used method for the investigation of different

phases of the cell cycle. A flow cytometer (BD accuri C6 cytometer) was used for the cell cycle analysis. A549 cells were treated with a corresponding IC_{50} dose of as-prepared ZnO NPs (L5/L10) for 48 h. Concisely, about $1x10^6$ cells were harvested and resuspended in PBS. The resuspended solution was centrifuged, and the obtained pellet was fixed with 70% chilled alcohol prepared in PBS. Then, incubation of cells was done for 60 min at −20 °C followed by washing of samples twice with PBS and again incubated in a staining solution containing 200 μL of PI and 50 μL of RNase solution. Finally, samples were again incubated in dark for 30 min at room temperature (RT).

2.8. Statistical analysis

All cytotoxic results on A549 cell lines were analysed with one way ANOVA followed by Dunnett's multiple comparison tests. The Graphpad Prism 6 version software was used and $p < 0.05$ was considered statistically significant.

3. Results and discussions

3.1. Powder X-ray diffraction (PXRD)

Fig. 1 shows the PXRD pattern of as-prepared ZnO NPs (L5/L10) and Table 1 shows 2θ values of corresponding diffraction peaks with respect to the Miller indices (*hkl*) planes. The obtained pattern is well matched with the wurtzite crystalline structure (hexagonal phase) JCPDS # 36–1451 [37,38]. Additionally, the intense and sharp peaks ascertain the perfect crystalline structure of the as-synthesized ZnO NPs. Moreover, no impurity peak is observed confirming the phase purity of ZnO NPs (i.e., absence of any secondary phase).

3.2. UV–visible analysis

The formation of ZnO NPs is also confirmed by UV–vis spectroscopy. Fig. 2(a) shows the absorption spectra of the as-synthesized ZnO NPs (L5/L10) while Fig. 2(b) and (c) represent corresponding tauc plots of L5 and L10 NPs, respectively. The maximum absorption peaks for L5 and L10 are obtained at 350 nm and 270 nm, respectively. The absorbance peak can be attributed to the intrinsic bandgap of ZnO due to the transition of electrons from the valence band to the conduction band [39]. A similar absorbance peak position of ZnO NPs has been reported by various researchers [40–42]. Furthermore, the corresponding bandgap energy for L5 and L10 is calculated as 2.26 eV and 2.60 eV using the tauc plots as shown in Fig. 2(b) and (c), respectively which is similar to the reported bandgap energy value of 2.6 eV for ZnO NPs [43].

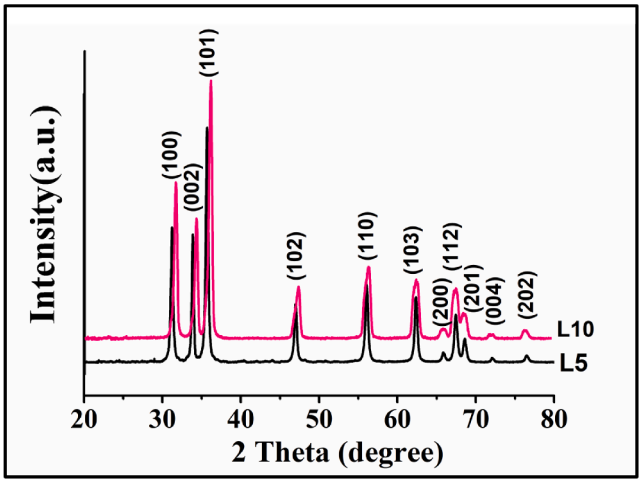

Fig. 1. PXRD pattern of the biosynthesized ZnO nanoparticles (L5 and L10).

Table 1
Represents the 2θ values of the observed diffraction peaks of the biosynthesized ZnO nanoparticles (L5 and L10) and corresponding miller indices planes.

S. No.	2θ (L5)	2θ (L10)	(*hkl*)
1.	31.22	31.70	100
2.	33.88	34.40	002
3.	35.72	36.20	101
4.	46.98	47.50	102
5.	56.1	56.50	110
6.	62.34	62.58	103
7.	65.84	65.92	200
8.	67.44	67.54	112
9.	68.58	68.68	201
10.	72.16	72.26	004
11.	76.48	76.70	202

3.3. FT-IR analysis

The presence of phytochemicals coatings attached to the surface of biosynthesized ZnO NPs are identified by FT-IR spectroscopy. Fig. 3 depicts the FT-IR spectrum of as-synthesized ZnO NPs (L5/L10). The peaks at 906.37 cm^{-1}, 838.88 cm^{-1}, 842.73 cm^{-1},713.53 cm^{-1}, 711.60 cm^{-1}, 617.10 cm^{-1} and 615.18 cm^{-1} can be associated to numerous phytochemicals (aromatics) present in the aqueous leaf extract of *Azadirachta indica* [44]. The corresponding bands at around 3494.38 cm^{-1}, 3407.6 cm^{-1}, and 3208.96 cm^{-1} are related to O—H stretching and the bands at 1504.20 cm^{-1} and 1446.35 cm^{-1} are associated with O—H bending, while 1417.42 cm^{-1} bands conforming to C═C stretching mode in aromatic compounds. In addition, 1031.73 cm^{-1}, and 1116.58 cm^{-1} bands are assigned to C—O stretching modes and 1105.01 cm^{-1} bands are correlated to C—N stretching of amines respectively [45,46]. Moreover, the bands obtained at 539.97 cm^{-1} and 478.25 cm^{-1} can be associated with Zn—O stretching.

3.4. TGA analysis

Fig. 4 depicts the TGA curves of the biosynthesized ZnO NPs (L5/L10). It can be seen that major weight losses occurred in two stages. The first weight loss occurred in the temperature range of ~35–103 °C due to evaporation of physically adsorbed moisture and the second weight loss occurred in the temperature range of ~103–400 °C attributed to the decomposition of phytochemicals coatings which are attached to the surface of ZnO NPs [44,47]. After that, again % mass loss is occurring up to 900 °C continuously similar to the TGA results reported by Moharram et al. [48]. It is estimated from the TGA result that the amount of the phytochemicals coatings capped to the surface of ZnO NPs is 87.15 wt% in L5 and 90.58 wt% in L10.

3.5. FE-SEM analysis

The FE-SEM micrographs of the prepared ZnO nanoparticles (L5 and L10) are presented in Fig. 5. The FE-SEM micrograph of L5 (Fig. 5(A)) shows the rod shape morphology with hexagonal ends with a diameter in the range of ~50–120 nm. Whereas the FE-SEM micrographs of L10 (Fig. 5 (A) and (C)) show the twisted rod shape morphology where ZnO nanorods with a diameter in the range of ~30–70 nm. Moreover, as-prepared L10 nanorods are thinner and more agglomerated compared to as-synthesized L5 nanorods which are found to be relatively well dispersed. Similar rod shape morphology has also been reported by several authors [49–51].

3.6. DLS/Zeta analysis

Figs. 6 and 7 revealed the plots of hydrodynamic sizes and the zeta potential graphs of the biosynthesized ZnO nanoparticles (L5 and L10), respectively. The hydrodynamic sizes (D_h) are determined as 580.41 nm

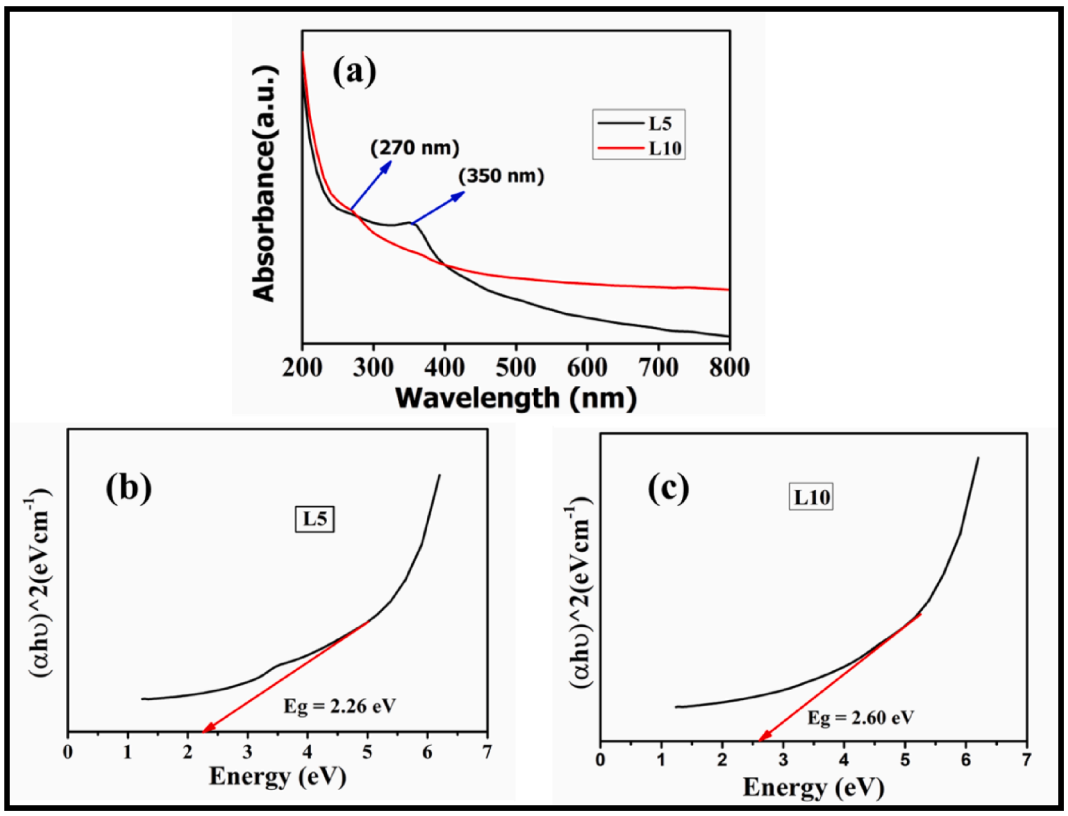

Fig. 2. UV– visible absorbance spectrum (a) and corresponding tauc plots (b and c) of the biosynthesized ZnO nanoparticles (L5 and L10), respectively.

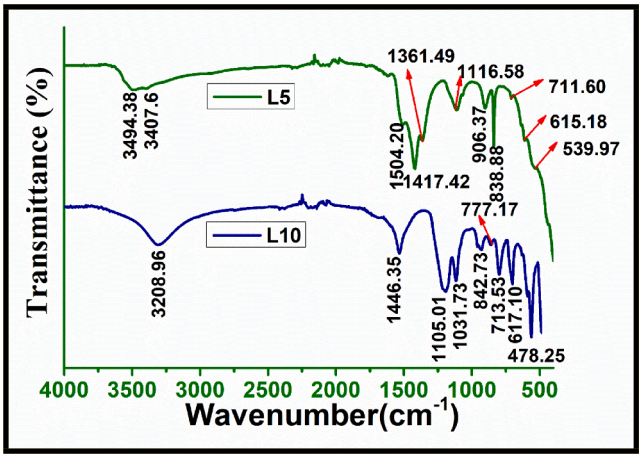

Fig. 3. FT-IR spectrum of the biosynthesized ZnO nanoparticles (L5 and L10).

and 356.2 nm for L5 and L10 NPs, respectively. The larger D_h values of biosynthesized L5/L10 NPs can be related to the interactions of surface-attached phytochemicals onto the surface of ZnO NPs nanoparticles in their aqueous suspension [47,52]. Furthermore, L5 NPs revealed a higher D_h value due to a larger amount of surface-attached phytochemicals coatings (determined by TGA) than that of L10 NPs. Zeta potential (ζ) values are measured as −47.17 mV and −51.70 mV for L5 and L10 NPs, respectively. A similar ζ value of −44 mV has been reported by Alyamani et al. for ZnO NPs biosynthesized using *Phlomis* leaf extract [53]. Likewise, Eltarahony et al reported the ζ value of −53.4 mV for the biosynthesized ZnO NPs [54]. Moreover, negative ζ values (below −30 mV) of L5/L10 indicate high colloidal stability of the biosynthesized ZnO NPs in aqueous suspension [55,56].

3.7. Effect of biosynthesized ZnO NPs (L5/L10) on the viability of A549 cells

MTT assay was carried out to examine the effect of biosynthesized ZnO NPs on the viability of lung cancer (A549) cells using different concentrations of L5/L10 NPs. The OD value was recorded at 570 nm using the microplate reader. The number of live cells was reflected in the absorbance value at two different time intervals (24 h and 48 h). The larger OD value indicates a greater number of live cells. Fig. 8(a) and (c) depicts the OD values of the A549 cells treated with L5 and L10 NPs at various concentrations (100, 150, 200 and 250 μg/mL) of ZnO NPs up to 48 h time intervals, respectively. Fig. 8(b) and (d) represent the corresponding cell viability graphs for L5 and L10 NPs, respectively.

It can be seen that the viability of A549 cells decreases with the increase in the concentration of L5/L10 nanoparticles (in a dose-dependent manner in both cases). It can be also observed that cell viability is significantly reduced at an incubation period of 48 h at the various concentrations (100, 150, 200 and 250 μg/mL) of ZnO nanoparticles. Moreover, the obtained IC_{50} values are determined as 125.64 μg/mL and 115.63 μg/mL at 48 h incubation for L5 and L10 NPs, respectively. Similar studies are reported by other groups using biosynthesized ZnO nanoparticles on different cancer cell lines [57,58].

3.8. Effect of biosynthesized ZnO NPs (L5/L10) on the morphology of A549 cells

The effect of biosynthesized ZnO NPs (L5/L10) on the morphology of A549 cells is investigated via a crystal violet assay where the cells were imaged at 200× magnification in an upright microscope (Nikon) after staining them using a crystal violet. Fig. 9 (a) and (b) represent the crystal violet stained micrographs of A549 cells treated with L5 and L10 ZnO nanoparticles, respectively and their comparison with the cells treated with chemically synthesized ZnO NPs (reported earlier [59]). In the case of L5 ZnO NPs, the cells were treated with IC_{50} dose (125.64 μg/

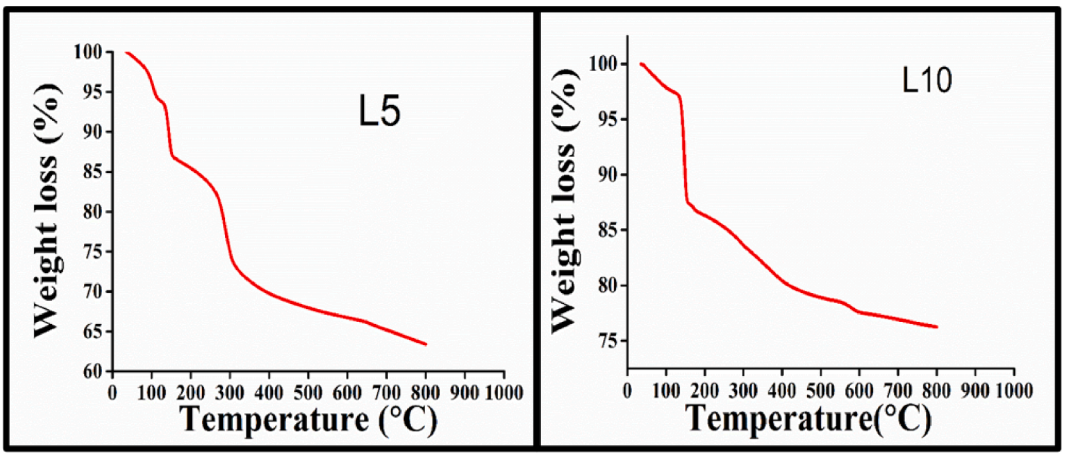

Fig. 4. TGA curves of the biosynthesized ZnO nanoparticles (L5 and L10).

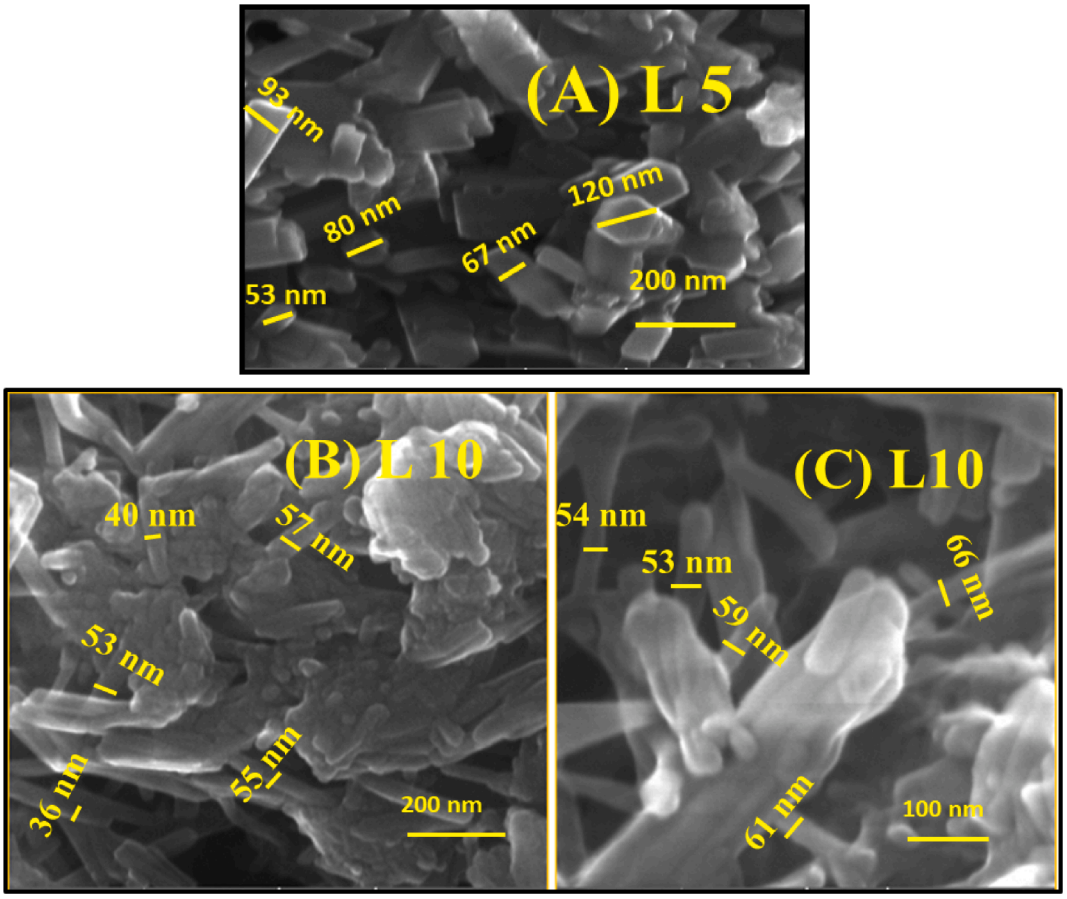

Fig. 5. FE-SEM micrographs of the biosynthesized ZnO NPs: (A) for L5 shown in (A) and (B), (C) for L10 (yellow coloured Text labelling is uniform for all three images).

mL) whereas in the case of L10 ZnO NPs, the cells were treated with IC_{50} dose (115.63 μg/mL) respectively for 48 h. It can be predicted that shrinkage of cells that was accompanied by rounded cell morphology, reduced cell number and poor cell adhesion are occurred due to the treatment L5/L10 NPs. Moreover, it can be also predicted that L10 ZnO NPs have higher anticancer effect on the morphology of A549 cells than L5 ZnO NPs.

3.9. Induction of apoptosis in A549 cells by biosynthesized ZnO NPs (L5 and L10)

It is reported that anticancer activity of biosynthesized metal oxide nanoparticles (MONPs) is occurred due to the induction of apoptosis [60]. The main reason behind the induction of apoptosis is the generation of reactive oxygen species (ROS) by MONPs. The increase in ROS leads to oxidative stress. In response to this oxidative stress, protein denaturation and lipid peroxidation occurred. This is then followed by DNA damage and necrosis, which leads to cell death by apoptosis [61].

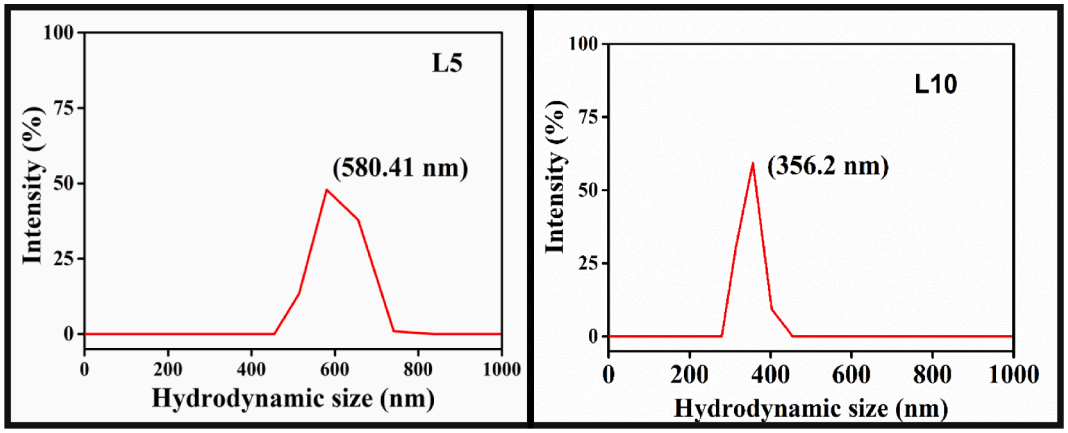

Fig. 6. DLS plots of hydrodynamic sizes obtained for the biosynthesized ZnO nanoparticles (L5 and L10).

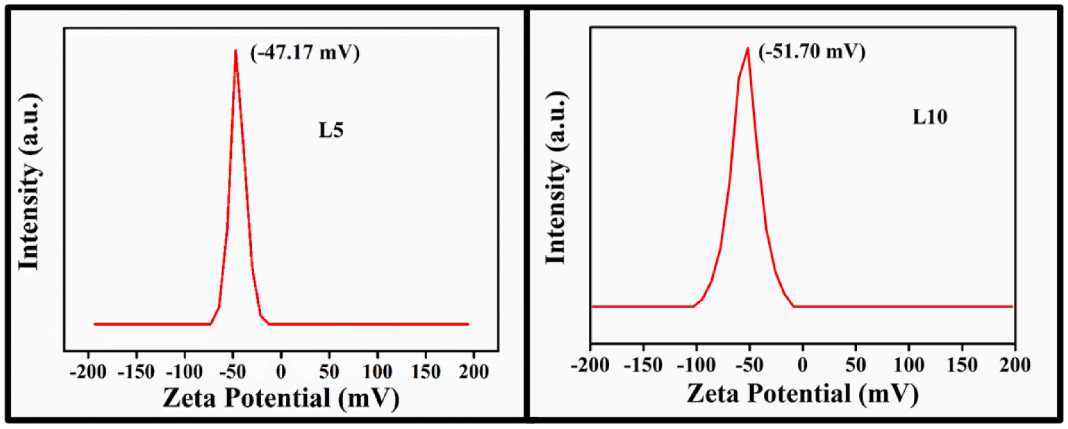

Fig. 7. Zeta potential of the biosynthesized ZnO nanoparticles (L5 and L10).

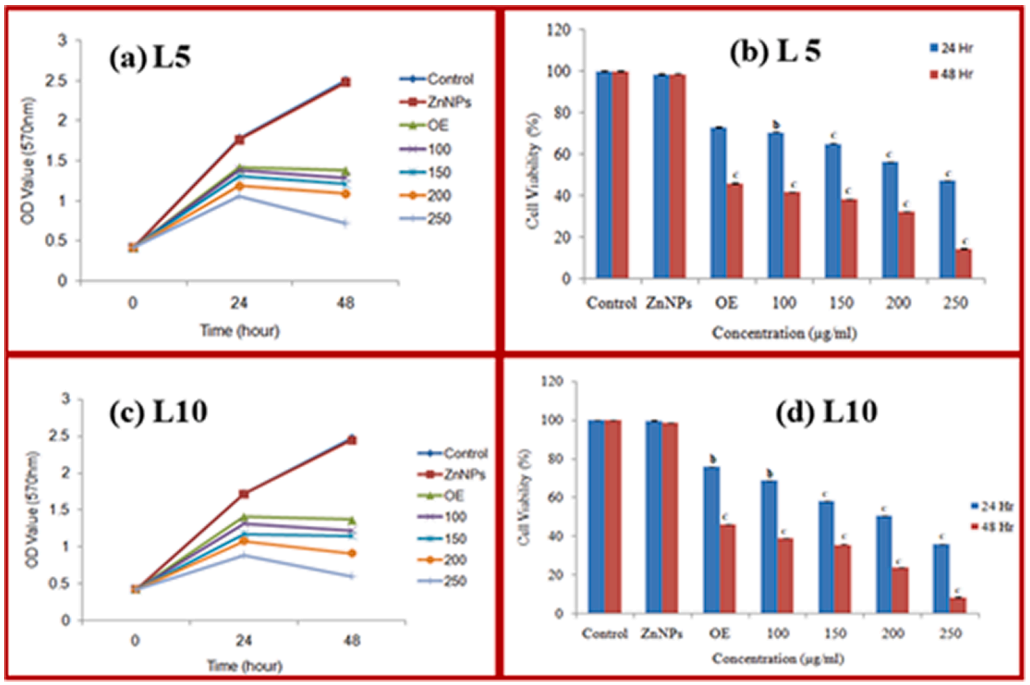

Fig. 8. (a) and (c) depict the OD values of A549 cells treated with L5 and L10 NPs, respectively at different concentrations (100, 150, 200 and 250 µg/mL) of ZnO NPs and at two different time intervals (24 h and 48 h). Data is represented in triplicate by performing three separate experiments. Fig. 8. (b) and (d) represent the corresponding cell viability of A549 cells treated with L5 and L10 NPs, respectively. Data are represented as mean ± SD. ($p \leq 0.05^{a}$, $p \leq 0.01^{b}$, $p \leq 0.001^{c}$).

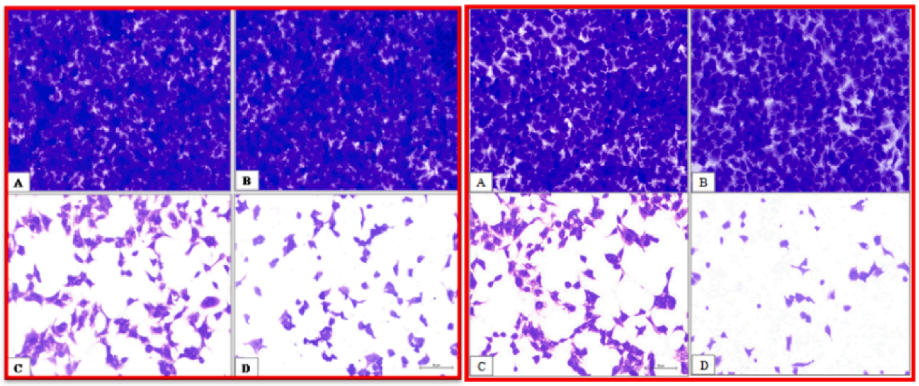

Fig. 9. (a) and (b) represents the morphology of human lung cancer A549 cells treated with L5 and L10, respectively. (A) No treatment (Control group), (B) Cells treated with ZnO NPs synthesized using wet chemical method (reported earlier [59]), (C) Cells treated with only leaf extract, (D) Cells treated with biosynthesized ZnO NPs (L5/L10) using leaf extract with corresponding IC_{50} dose, at 200x magnification.

Moreover, Sulaiman et al. also reported that the induction of apoptosis by biosynthesized iron oxide nanoparticles occurred due to disruptions in mitochondrial-mediated apoptotic pathways [62]. The occurrence of apoptosis can be confirmed by looking carefully at the specific changes that occurred in the morphological characterizations of cells. These specific changes include cell shrinkage, chromatin condensation, and cytoplasmic or nuclear fragmentations. To confirm the induction of apoptosis in A549 cells, an acridine orange (AO) and propidium iodide (PI) dual staining study was done. PI staining can display dead cells whereas AO staining can exhibit healthy cells or early apoptotic cells with fragmented DNA. Fig. 10 (a) and (b) represent the fluorescent (AO/PI) micrographs of A549 cells treated with biosynthesized ZnO NPs with a corresponding IC_{50} dose (125.64 μg/mL) of L5 and IC_{50} dose (115.63 μg/mL) of L10, respectively and their comparison with the cells treated with chemically synthesized ZnO NPs (reported earlier [59]). After that, the A549 cells were visualised under a fluorescent microscope (Nikon) to analyse viable cells, early apoptosis and late apoptosis phases.

We have observed indications of cell death such as early apoptosis, secondary necrosis and chromatin condensations for A549 cells treated with both L5 and L10 NPs. The presence of green coloured intact nuclei in the untreated A549 cells confirmed the presence of viable cells (VC) after 48 h (i.e. cell is healthy and it has not undergone any changes like apoptosis, or necrosis). Moreover, early apoptosis (EA) and secondary necrosis (SN) stages were seen for both cases at corresponding IC_{50} doses of L5 and L10 NPs. The indication of these morphological changes confirmed the induction of apoptosis in A549 cells treated with biosynthesized ZnO NPs (L5 and L10).

3.10. Cell cycle analysis by flow cytometry

Cell cycle analysis was conducted to examine the interfering ability of biosynthesized ZnO NPs (L5 and L10) with the cell cycle pattern. Furthermore, to investigate the distribution of cell cycle phases in A549 cells treated with both L5 and L10 NPs, flow cytometry analysis was carried out after 48 h exposure with IC_{50} dose of both ZnO NPs. Fig. 11 (a) and (b) depict flow cytometry analysis of cell cycle arrest in A549

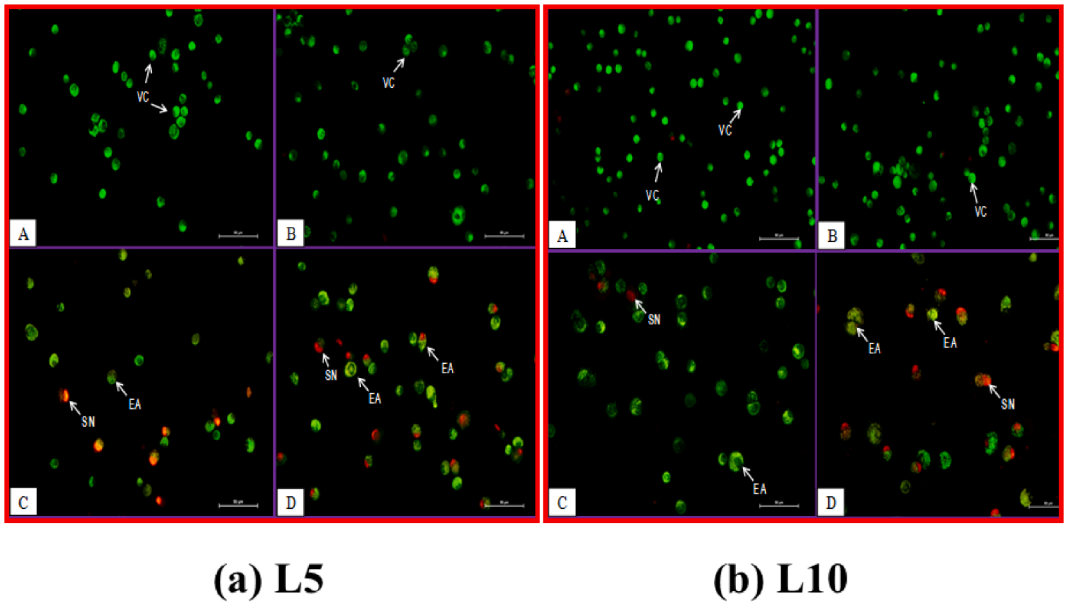

Fig. 10. Apoptosis and morphological analysis of A549 cells treated with (a) L5 and (b) L10 NPs and double-stained with AO and PI as observed under a fluorescent microscope (Nikon): (A) Cells without treatment, (B) Cells treated with ZnO NPs synthesized using wet-chemical method (reported earlier [59]), (C) Cells treated with only leaf extract, (D) Cells treated with biosynthesized ZnO NPs (L5/L10) using leaf extract with corresponding IC_{50} dose (where EA: early apoptosis; VC: viable cells and SN: secondary necrosis).

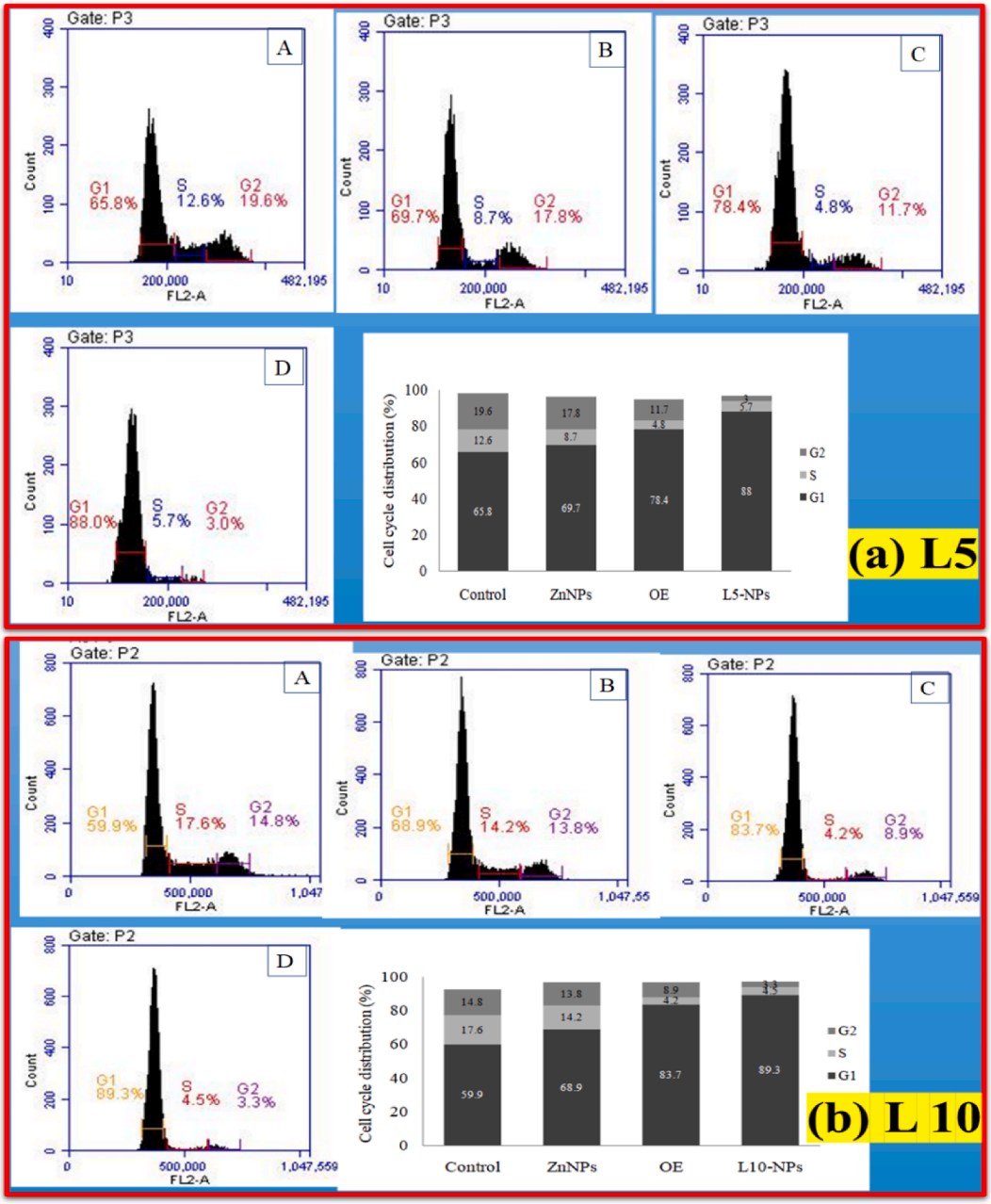

Fig. 11. Flow cytometry analysis of cell cycle arrest in A549 cells treated with (a) 125.64 μg/mL of L5 and (b) 115.63 μg/mL of L10 NPs for 48 h. The percentage distributions of the cell cycle are shown in the bar diagram. (A) Cells without treatment, (B) Cells treated with ZnO NPs synthesized using wet-chemical method (reported earlier [57]), (C) Cells treated with only leaf extract, (D) Cells treated with biosynthesized ZnO NPs (L5/L10) using leaf extract with corresponding IC_{50} dose.

cells treated with biosynthesized ZnO NPs on exposure to IC_{50} dose of 125.64 μg/mL of L5 and 115.63 μg/mL of L10 NPs for 48 h, respectively. Moreover, Table 2 represents the % of cell cycle phase arrest by both biosynthesized ZnO NPs (L5 and L10). It can be seen that 88 % and 89.3 % of arrests of the G1 phase of the cell cycle occurred due to the anticancer effect of L5 and L10 NPs, respectively. Shamasi et al. have reported the importance of *Rubia tinctorum-mediated* ZnO nanoparticles in the induction of apoptosis against MCF-7 cell lines [63]. They have revealed an increase in % of cells in the G1 phase from 30% to 80 % when they are treated with increased concentration of biosynthesized ZnO nanoparticles. Likewise, Yakop et al. have studied the apoptotic activity of silver nanoparticles which were synthesized using *Clinacanthus Nutans* leaf extract [64]. They have observed significant changes in the G1 phase of the HSC-4 cell lines when treated with biosynthesized silver nanoparticles. The authors also demonstrated from the flow cytometry results that the % of G1 phase of the HSC-4 cell lines increases from 58.63% ± 1.15 to 85.83% ± 2.68 because of their treatment with the biosynthesized silver nanoparticles at an increase of incubation time (i.e., from 2 h to 4 h).

Table 2
The cell cycle phase arrest by the green synthesized zinc oxide nanoparticles (L5 and L10).

S. No.	Cell cycle phase	ZnO (L5)	ZnO (L10)
1	G1 phase	88.0%	89.3%
2	S phase	5.7%	4.5%
3	G2 phase	3.0%	3.3%

4. Conclusion

In this present work, we have successfully biosynthesized ZnO nanorods in an inexpensive and eco-friendly manner. Herein, 50–120 and 30–70 nm rod-shaped L5 and L10 NPs are synthesized using 5 mL and 10 mL leaf extract of *Azadirachta indica* (Neem tree), respectively. As-prepared L5/L10 has revealed a pure hexagonal wurtzite (crystalline) structure and their surface is attached with phytochemicals coating with the amount of 12.85 wt% in L5 and 9.42 wt% in L10. DLS study showed hydrodynamic sizes 580.41/356.2 nm and zeta potential values of −47.17/−51.70 mV for L5/L10, respectively indicating their good colloidal stability in an aqueous suspension. The anticancer activity of as-synthesized ZnO NPs (L5/L10) is evaluated on A549 lung cancer cell lines via MTT, crystal violet, and flow cytometry assay. MTT assay revealed the IC_{50} values of biosynthesized ZnO nanoparticles as 125.64 μg/mL for L5 and 115.63 μg/mL for L10, respectively. As the amount of leaf extract increased for biosynthesis, we observed a more cytotoxic effect (as indicated by the lower value of IC_{50} in the case of L10) by the ZnO nanoparticles. Moreover, the flow cytometry study depicted the arrest of the G1 cell cycle phase of 88% with L5 and 89.3% with L10 NPs, respectively. Thus, biosynthesized ZnO nanorods (L5/L10) have great potential to be applied as promising clinical therapeutic agents for lung cancer treatment. However, prior knowledge of the mechanism involved in the plant-mediated biosynthesis of ZnO NPs and in vivo extensive experimental research is required to make the approach economically more favourable.

5. Disclosure

The authors declare no conflicts of interest for publishing this research work.

Declaration of Competing Interest

The authors declare that they have no known competing financial interests or personal relationships that could have appeared to influence the work reported in this paper.

Acknowledgement

We would like to show our gratitude to the Principal, Miranda House, University of Delhi for providing the lab facility to carry out this research work. The authors would like to thank USIC, University Scientific Instrumentation Centre, University of Delhi, India for providing facilities like FT-IR, PXRD and FE-SEM. D. Maity would like to thank the University of Petroleum and Energy Studies (UPES) for providing SEED Funding (UPES/R&D-HS/24022022/08) and all other supports.

References

[1] Z.U. Abideen, A.H. Shah, F. Teng, M.I. Abro, K. Ullah, One-step hydrothermal synthesis of ZnO microtubes with an efficient photocatalytic activity, Micro Nano Lett. 2 (2021) 142–148, https://doi.org/10.1049/mna2.12024.

[2] S. Arya, P. Mahajan, S. Mahajan, A. Khosla, R. Datt, V. Gupta, S. J. Young, S. K. Oruganti, Influence of processing parameters to control morphology and optical properties of Sol-Gel synthesized ZnO nanoparticles ECS J. Solid State Sci. Technol. 10(2) (2021) 023002. doi:10.1149/ 2162-8777/abe095.

[3] A. Manohar, J. Park, D.D. Geleta, C. Krishnamoorthi, R. Thangam, H. Kang, J. Lee, Synthesis and characterization of ZnO nanoparticles for photocatalysis, antibacterial and cytotoxicity in kidney cancer (A498) cell lines, J. Alloys Compd. 874 (2021) 159868, https://doi.org/10.1016/j.jallcom.2021.159868.

[4] M.S. Choi, H.G. Na, G.S. Shim, J.H. Cho, M.Y. Kim, S.I. Kim, S.H. Baek, C. Jin, K. H. Lee, Simple and scalable synthesis of urchin-like ZnO nanoparticles via a microwave-assisted drying process, Ceram. Int. 47 (10) (2021) 14621–14629, https://doi.org/10.1016/j.ceramint.2021.02.045.

[5] S. Wirunchit, P. Gansa, W. Koetniyom, Synthesis of ZnO nanoparticles by Ball-milling process for biological applications, Mater. Today: Proc. 47 (2021) 3554–3559, https://doi.org/10.1016/j.matpr.2021.03.559.

[6] B. Manikandan, T. Endo, S. Kaneko, K.R. Murali, R. John, Properties of sol gel synthesized ZnO nanoparticles, J. Mater. Sci. Mater. Electron. 29 (11) (2018) 9474–9485, https://doi.org/10.1007/s10854-018-8981-8.

[7] D. Garibo, H.A. Borbón-Nuñez, J.N.D. de León, E. García Mendoza, I. Estrada, Y. Toledano-Magaña, H. Tiznado, M. Ovalle-Marroquin, A.G. Soto-Ramos, A. Blanco, J.A. Rodríguez, Green synthesis of silver nanoparticles using Lysiloma acapulcensis exhibit high-antimicrobial activity, Sci. Rep. 10 (1) (2020) 1–11, https://doi.org/10.1038/s41598-020-69606-7.

[8] S. Jadoun, R. Arif, N.K. Jangid, R.K. Meena, Green synthesis of nanoparticles using plant extracts: a review, Environ. Chem. Lett. 19 (1) (2021) 355–374, https://doi.org/10.1007/s10311-020-01074-x.

[9] R.S. Sathishkumar, A. Sundaramanickam, R. Srinath, T. Ramesh, K. Saranya, M. Meena, P. Surya, Green synthesis of silver nanoparticles by bloom forming marine microalgae *Trichodesmium erythraeum* and its applications in antioxidant, drug-resistant bacteria, and cytotoxicity activity, J. Saudi Chem. Soc. 23 (8) (2019) 1180–1191, https://doi.org/10.1016/j.jscs.2019.07.008.

[10] R. Raliya, J.C. Tarafdar, ZnO nanoparticle biosynthesis and its effect on phosphorous-mobilizing enzyme secretion and gum contents in clusterbean (Cyamopsis tetragonoloba L.), Agric. Res. 2 (1) (2013) 48–57.

[11] P. Karpagavinayagam, C. Vedhi, Green synthesis of iron oxide nanoparticles using *Avicennia marina* flower extract, Vacuum 160 (2019) 286–292, https://doi.org/10.1016/j.vacuum.2018.11.043.

[12] N.K. Gour, Jain, Advances in green synthesis of nanoparticles, Artif. Cells Nanomed. Biotechnol. 47 (1) (2019) 844–851, https://doi.org/10.1080/21691401.2019.1577878.

[13] V. Selvanathan, M. Aminuzzaman, L.H. Tey, S.A. Razali, K. Althubeiti, H. I. Alkhammash, S.K. Guha, S. Ogawa, A. Watanabe, M. Shahiduzzaman, M. Akhtaruzzaman, *Muntingia calabura* leaves mediated green synthesis of CuO nanorods: exploiting phytochemicals for unique morphology, Materials 14 (21) (2021) 6379, https://doi.org/10.3390/ma14216379.

[14] L. Kaliraj, J.C. Ahn, E.J. Rupa, S. Abid, J. Lu, D.C. Yang, Synthesis of panos extract mediated ZnO nano-flowers as photocatalyst for industrial dye degradation by UV illumination, J. Photochem. Photobiol. B: Biol. 199 (2019) 111588, https://doi.org/10.1016/j.jphotobiol.2019.111588.

[15] F.T. Thema, E. Manikandan, A. Gurib-Fakim, M. Maaza, Single phase Bunsenite NiO nanoparticles green synthesis by *Agathosma betulina* natural extract, J. Alloys Compd. 657 (2016) 655–661, https://doi.org/10.1016/j.jallcom.2015.09.227.

[16] B. Ahmmad, K. Leonard, M.S. Islam, J. Kurawaki, M. Muruganandham, T. Ohkubo, Y. Kuroda, Green synthesis of mesoporous hematite (α-Fe2O3) nanoparticles and their photocatalytic activity, Adv. Powder Technol. 24 (1) (2013) 160–167, https://doi.org/10.1016/j.apt.2012.04.005.

[17] M. Hudlikar, S. Joglekar, M. Dhaygude, K. Kodam, Green synthesis of TiO2 nanoparticles by using aqueous extract of *Jatropha curcas* L. latex, Mater. Lett. 75 (2012) 196–199, https://doi.org/10.1016/j.matlet.2012.02.018.

[18] H.R. Naika, K. Lingaraju, K. Manjunath, D. Kumar, G. Nagaraju, D. Suresh, H. Nagabhushana, Green synthesis of CuO nanoparticles using Gloriosa superba L. extract and their antibacterial activity, J. Taibah Univ. Sci. 9 (1) (2015) 7–12, https://doi.org/10.1016/j.jtusci.2014.04.006.

[19] T.U.D. Thi, T.T. Nguyen, Y.D. Thi, K.H.T. Thi, B.T. Phan, K.N. Pham, Green synthesis of ZnO nanoparticles using orange fruit peel extract for antibacterial activities, RSC Adv. 10 (40) (2020) 23899–23907, https://doi.org/10.1039/D0RA04926C.

[20] U.R. Sharma, N. Sharma, Green synthesis, anti-cancer and corrosion inhibition activity of Cr2O3 nanoparticles, Biointerf. Res. Appl. Chem 11 (2021) 8402–8412, https://doi.org/10.33263/BRIAC111.84028412.

[21] K.C. Suresh, S. Surendhiran, P. Manoj Kumar, E. Ranjth Kumar, Y.A. Khadar, A. Balamurugan, Green synthesis of SnO2 nanoparticles using Delonix elata leaf extract: evaluation of its structural, optical, morphological and photocatalytic properties, SN Appl. Sci. 2 (10) (2020) 1–13, https://doi.org/10.1007/s42452-020-03534-z.

[22] J. Fall, N. Sackey, B.D. Mayedwa, Ngom, Investigation of structural and optical properties of CdO nanoparticles via peel of Citrus x sinensis, Mater. Today: Proc. 36 (2021) 298–302, https://doi.org/10.1016/j.matpr.2020.04.057.

[23] H.E.A. Mohamed, K. Hkiri, M. Khenfouch, S. Dhlamini, M. Henini, M. Maaza, Optical properties of biosynthesized nanoscaled Eu 2 O 3 for red luminescence applications, J. Opt. Soc. Am. A: Opt. Image Sci. Vis., 37(11) (2020) C73-C79. 10.1364/JOSAA.396244.

[24] Y.B. Hahn, Zinc oxide nanostructures and their applications, Korean J. Chem Eng. 28 (9) (2011) 1797–1813, https://doi.org/10.1007/s11814-011-0213-3.

[25] P. Król, K. Pomastowski, V. Rafińska, B. Railean-Plugaru, Buszewski, Zinc oxide nanoparticles: synthesis, antiseptic activity and toxicity mechanism, Adv. Colloid Interface Sci. 249 (2017) 37–52, https://doi.org/10.1016/j.cis.2017.07.033.

[26] P. Vishnukumar, S. Vivekanandhan, M. Misra, A.K. Mohanty, Recent advances and emerging opportunities in phytochemical synthesis of ZnO nanostructures, Mater. Sci. Semicond. Process 80 (2018) 143–161, https://doi.org/10.1016/j.mssp.2018.01.026.

[27] M. El Golli, N. Fendrich, C. Bazzanella, A. Dridi, M. Miotello, Orlandi, Wastewater remediation with ZnO photocatalysts: green synthesis and solar concentration as an economically and environmentally viable route to application, J. Environ. Manage. 286 (2021) 112226, https://doi.org/10.1016/j.jenvman.2021.112226.

[28] G. Rashidian, C.C. Lazado, H.H. Mahboub, R. Mohammadi-Aloucheh, M.D. Prokić, H.S. Nada, C. Faggio, Chemically and green synthesized ZnO nanoparticles alter key immunological molecules in common carp (Cyprinus carpio) skin mucus, Int. J. Mol. Sci. 22 (6) (2021) 3270, https://doi.org/10.3390/ijms22063270.

[29] M.D. Jayappa, C.K. Ramaiah, M.A.P. Kumar, D. Suresh, A. Prabhu, R.P. Devasya, S. Sheikh, Green synthesis of zinc oxide nanoparticles from the leaf, stem and in vitro grown callus of Mussaenda frondosa L.: characterization and their applications, Appl. Nanosci., 10(8) (2020) 3057-3074. 10.1007/s13204-020-01382-2.

[30] G. Sharmila, M. Thirumarimurugan, C. Muthukumaran, Green synthesis of ZnO nanoparticles using *Tecoma castanifolia* leaf extract: characterization and evaluation of its antioxidant, bactericidal and anticancer activities, Microchem. J. 145 (2019) 578–587, https://doi.org/10.1016/j.microc.2018.11.022.
[31] K. Selvam, A.A. Allam, J.S. Ajarem, C. Sudhakar, T. Selvankumar, B. Senthilkumar, W. Kim, *Annona reticulata* leaves-assisted synthesis of zinc oxide nanoparticles and assessment of cytotoxicity and photocatalytic impact, Mater. Lett. 309 (2022) 131379, https://doi.org/10.1016/j.matlet.2021.131379.
[32] S. Ali, K.G. Sudha, G. Karunakaran, M. Kowsalya, E. Kolesnikov, M.V. Gorshenkov, T. Velmurugan, M.P. Rajeshkumar, Anticancer and photocatalytic activities of zinc oxide nanorods synthesized from *Manilkara littoralis* leaf extract, Mater. Chem. Phys. 277 (2022) 125541, https://doi.org/10.1016/j.matchemphys.2021.125541.
[33] Annapoorani, A. Koodalingam, M. Beulaja, G. Saiprasad, P. Chitra, A. Stephen, S. Palanisamy, N.M. Prabhu, S. You, S. Janarthanan, R. Manikandan, Eco-friendly synthesis of zinc oxide nanoparticles using *Rivina humilis* leaf extract and their biomedical applications, Process Biochem. 112 (2022) 192–202, https://doi.org/10.1016/j.procbio.2021.11.022.
[34] S.K. Srivastava, B. Agrawal, A. Kumar, A. Pandey, Phytochemicals of Azadirachta Indica source of active medicinal constituent used for cure of various diseases: a review, J. Sci. Res. 64 (1) (2020) 385–390, https://doi.org/10.37398/JSR.2020.640153.
[35] S.P. Dash, S. Dixit, S. Sahoo, Phytochemical and biochemical characterizations from leaf extracts from *Azadirachta Indica*: an important medicinal plant, Biochem. Anal. Biochem. 6 (323) (2017) 2161–11009, https://doi.org/10.4172/2161-1009.1000323.
[36] R. Subapriya, S. Nagini, Medicinal properties of neem leaves: a review, Curr. Med. Chem.-Anti-Cancer Agents 5 (2) (2005) 149–156, https://doi.org/10.2174/1568011053174828.
[37] P. Saravanan, K. SenthilKannan, R. Divya, M. Vimalan, S.Tamilselvan, D. Sankar, A perspective approach towards appreciable size and cost-effective solar cell fabrication by synthesizing ZnO nanoparticles from *Azadirachta indica* leaves extract using domestic microwave oven, J. Mater. Sci.: Mater. Electron. 31(5) (2020) 4301–4309. doi:10.1007/s10854-020-02985-9.
[38] A.A. Barzinjy, H.H. Azeez, Green synthesis and characterization of zinc oxide nanoparticles using *Eucalyptus globulus* Labill. leaf extract and zinc nitrate hexahydrate salt, SN Appl. Sci. 2 (2020) 991. doi:10.1007/s42452-020-2813-1.
[39] A.K. Zak, M.E. Abrishami, W.A. Majid, R. Yousefi, S.M. Hosseini, Effects of annealing temperature on some structural and optical properties of ZnO nanoparticles prepared by a modified sol–gel combustion method, Ceram. Int. 37 (1) (2011) 393–398, https://doi.org/10.1016/j.ceramint.2010.08.017.
[40] L.M. Jose, S. Kuriakose, S. Thomas, Fabrication characterization and in vitro antifungal property evaluation of biocompatible lignin-stabilized zinc oxide nanoparticles against selected pathogenic fungal strains, BioNanoSci 10 (2020) 583–596, https://doi.org/10.1007/s12668-020-00748-8.
[41] P. Mitra, D. Dutta, S. Das, T. Basu, A. Pramanik, A. Patra, Antibacterial and photocatalytic properties of ZnO–9-aminoacridine hydrochloride hydrate drug nanoconjugates, ACS Omega 3 (7) (2018) 7962–7970, https://doi.org/10.1021/acsomega.8b00568.
[42] T. Aqeel, H.F. Greer, Quantum-sized zinc oxide nanoparticles synthesised within mesoporous silica (SBA-11) by humid thermal decomposition of zinc acetate, Crystals 10 (2020) 549, https://doi.org/10.3390/cryst10060549.
[43] S. Bayrami, S.R. Alioghli, A. Pouran, A. Habibi-Yangjeh, S.R. Khataee, A facile ultrasonic-aided biosynthesis of ZnO nanoparticles using *Vaccinium arctostaphylos* L. leaf extract and its antidiabetic, antibacterial, and oxidative activity evaluation, Ultrason. Sonochem. 55 (2019) 57–66, https://doi.org/10.1016/j.ultsonch.2019.03.010.
[44] J. López-López, A. Tejeda-Ochoa, A. López-Beltrán, J. Herrera-Ramírez, P. Méndez-Herrera, Sunlight photocatalytic performance of ZnO nanoparticles synthesized by green chemistry using different botanical extracts and zinc acetate as a precursor, Molecules 27 (2022) 6, https://doi.org/10.3390/molecules27010006.
[45] S. Aiswarya Devi, M. Harshiny, S. Udaykumar, P. Gopinath, M. Matheswaran, Strategy of metal iron doping and green-mediated ZnO nanoparticles: dissolubility, antibacterial and cytotoxic traits, Toxicol. Res. 6(6) (2017) 854–865. doi:10.1039/c7tx00093f.
[46] Lateef, A.O. Adeeyo, Green synthesis and antibacterial activities of silver nanoparticles using extracellular laccase of lentinus edodes, Not. Sci. Biol. 7(4) (2015) 405–411. doi:10.15835/nsb749643.
[47] D. Maity, S.-G. Choo, J. Yi, J. Ding, J.-M. Xue, Synthesis of magnetite nanoparticles via a solvent-free thermal decomposition route, J. Magn. Magn. Mater. 321 (2009) 1256–1259, https://doi.org/10.1016/j.jmmm.2008.11.013.
[48] A. H. Moharram, S. A. Mansour, M. A. Hussein, M. Rashad, Direct Precipitation and characterization of ZnO Nanoparticles, J. Nanomater, 2014 (2014) Article ID 716210 10.1155/2014/716210.
[49] F.Z. Haque, N. Singh, P. Pandey, M.R. Parra, Study of Zinc Oxide nano/micro rods grown on ITO and glass substrates, Optik. 124 (2013) 4167–4171, https://doi.org/10.1016/j.ijleo.2012.12.052.
[50] A.P. Sachi, M. Singh, ThirumalFabrication of AgNi nano-alloy-decorated ZnO nanocomposites as an efficient and novel hybrid catalyst to degrade noxious organic pollutants, ACS Omega 6 (50) (2021) 34771–34782, https://doi.org/10.1021/acsomega.1c05266.
[51] S.S. Rakhunde, K.M. Gadave, D.R. Shinde, P.K. Bhujbal, Effect of dye absorption time on the performance of a novel 2-HNDBA sensitized ZnO photo anode based dye-sensitized solar cell, Eng. Sci. 12 (2020) 117–124, https://doi.org/10.30919/es8d1146.
[52] H. Mohd Yusof, N. Abdul Rahman, R. Mohamad, U.H. Zaidan, A.A. Samsudin, Biosynthesis of zinc oxide nanoparticles by cell-biomass and supernatant of *Lactobacillus plantarum* TA4 and its antibacterial and biocompatibility properties, Sci. Rep. 10 (1) (2020).
[53] A.A. Alyamani, S. Albukhaty, S. Aloufi, F.A. AlMalki, H. Al-Karagoly, G. M. Sulaiman, Green fabrication of zinc oxide nanoparticles using *Phlomis* leaf extract: characterization and in vitro evaluation of cytotoxicity and antibacterial properties, Molecules 26 (2021) 6140, https://doi.org/10.3390/molecules26206140.
[54] M. Eltarahony, S. Zaki, M. ElKady, D. Abd-El-Haleem, Biosynthesis, characterization of some combined nanoparticles, and its biocide potency against a broad spectrum of pathogens, J. Nanomater. 2018 (2018), https://doi.org/10.1155/2018/5263814.
[55] K. Ganeshlenin, A. Sudame, P. Bhati, A. Chakrabarty, S.N. Kale, D. Maity, Systematic magnetic fluid hyperthermia studies of carboxyl functionalized hydrophilic superparamagnetic iron oxide nanoparticles based ferrofluids, J. Colloid Interface Sci. 514 (2018) 534–543, https://doi.org/10.1016/j.jcis.2017.12.064.
[56] G. Kandasamy, S. Soni, K. Sushmita, N.S. Veerapu, S. Bose, D. Maity, One-step synthesis of hydrophilic functionalized and cytocompatible superparamagnetic iron oxide nanoparticles (SPIONs) based aqueous ferrofluids for biomedical applications, J. Mol. Liquids 274 (2019) 653–663, https://doi.org/10.1016/j.molliq.2018.10.161.
[57] S. Donga, S. Chanda, *Caesalpinia crista* seeds mediated green synthesis of zinc oxide nanoparticles for antibacterial, antioxidant, and anticancer activities, BioNanoSci. (2022) 1–12, https://doi.org/10.1007/s12668-022-00952-8.
[58] S. Khaleghi, J. Khayatzadeh, A. Neamati, Biosynthesis of Zinc Oxide nanoparticles using *Origanum majorana* L. leaf extract, its antioxidant and cytotoxic activities, Mater. Technol. (2022) 1–10, https://doi.org/10.1080/10667857.2022.2044218.
[59] N. Rani, K. Rawat, M. Saini, A. Shrivastava, G. Kandasamy, K. Saini, D. Maity, Rod-shaped ZnO nanoparticles: synthesis, comparison and in vitro evaluation of their apoptotic activity in lung cancer cells, Chem. Pap. 76 (2) (2022) 1225–1238, https://doi.org/10.1007/s11696-021-01942-y.
[60] N. Rani, K. Saini, K.,, Biogenic metal and metal oxides nanoparticles as anticancer agent: a review, in: IOP Conference Series: Materials Science and Engineering 1225 (1), 2022, p. 012043, https://doi.org/10.1088/1757-899X/1225/1/012043.
[61] M. Valko, C.J.B. Rhodes, J. Moncol, M.M. Izakovic, M. Mazur, Free radicals, metals and antioxidants in oxidative stress-induced cancer, Chem. Biol. Interact. 160 (1) (2006) 1–40, https://doi.org/10.1016/j.cbi.2005.12.009.
[62] G.M. Sulaiman, A.T. Tawfeeq, A.S. Naji, Biosynthesis, characterization of magnetic iron oxide nanoparticles and evaluations of the cytotoxicity and DNA damage of human breast carcinoma cell lines, Artif. Cells Nanomed. Biotechnol. 46 (6) (2018) 1215–1229, https://doi.org/10.1080/21691401.2017.1366335.
[63] Z. Shamasi, A. Es-haghi, M.E. Taghavizadeh Yazdi, M.S. Amiri, M. Homayouni-Tabrizi, Role of *Rubia tinctorum* in the synthesis of zinc oxide nanoparticles and apoptosis induction in breast cancer cell line, Nanomed. J. 8(1) (2021) 65–72. doi: 10.22038/ nmj.2021.08.07.
[64] F. Yakop, S.A.A. Ghafar, Y.K. Yong, L.S. Yazan, R.M. Hanafiah, V. Lim, Z. Eshak, Silver nanoparticles *Clinacanthus Nutans* leaves extract induced apoptosis towards oral squamous cell carcinoma cell lines, Artif. Cells Nanomed. Biotechnol. 46 (2) (2018) 131–139, https://doi.org/10.1080/21691401.2018.1452750.